Imaging the Mode-Selected Predissociation of $OCS^+[(v_1v_2v_3)\tilde{B}^2\Sigma^+]$

Chushuan Chang,† Chu-Yung Luo, and Kopin Liu*,†

Institute of Atomic and Molecular Sciences (IAMS), Academia Sinica, P.O. Box 23-166, Taipei, Taiwan 106

Received: November 11, 2004

A new experimental approach to explore the mode-selected chemistry is proposed and demonstrated here. In this approach a double-resonance excitation scheme is exploited to prepare a well-defined mode or state of a parent ion. A time-sliced velocity imaging technique interrogates the fragment ion from the subsequent predissociation. Application to the title process reveals remarkable mode-specific behaviors despite the long dissociation time associated with the indirect bond-breaking process. A qualitative interpretation of the major findings is surmised.

I. Introduction

Mode-specific and/or bond-selected chemistry is a fascinating subject for investigations.[1−3] Besides its potential application, the observation of this selectivity can lead to a better understanding of the mode couplings and intramolecular energy flow while a chemical bond is broken and formed. Pioneered by Crim,[1] Zare,[2] and others,[3] the past decade has witnessed a number of remarkable studies from which the concept of *active* and *conserved* modes as well as the *spectator* paradigm emerge. In those experiments a neutral parent molecule or one of the polyatomic reagents is first prepared in a particular vibrationally excited state by laser excitation; the subsequent vibrationally mediated photodissociation or reaction outcome is then probed. Because of the limitations of the initial preparation in this approach—requiring an IR- or Raman-active mode and the limited wavelength range of a typical preparation laser—not all vibrational modes/states can readily be accessed, rendering a complete mode-specific comparison impossible.

Reported here is an alternative experimental approach that enables us to scrutinize the full mode specificity in a given ionic system. To demonstrate its power and feasibility, we chose the predissociation process of $OCS^+(\tilde{B}\ ^2\Sigma^+)$ for illustration. As depicted in Figure 1, a state(s)-specific parent ion is initially prepared by a resonance-enhanced multiphoton ionization (REMPI) process. A second laser is fired after a short delay to induce the photodissociation of interest. The dynamical attributes of the predissociative fragment ions are then mapped by a newly developed, time-sliced velocity imaging technique.[5] The basic idea of this approach is simple: merely reversing the roles of the dissociation and ionization lasers in a typical pump-and-probe experiment. The use of REMPI to prepare state-selected ions is not totally new. For example, previously Anderson and co-workers[6,7] used REMPI to prepare a parent ion in a collision-induced dissociation experiment to examine the effects of mode(s)-specific vibrational excitation. Weinkauf and Boesl[8−10] combined REMPI and photofragmentation yield spectroscopy for studying the spectroscopy of electronic excited states of molecular ions. More recently, Ashfold and co-workers[11] applied velocity map ion imaging methods in studying the photofragmentation of a state-selected diatomic ion Br_2^+ in which a (2 + 1) REMPI process was used to select the initial state of Br_2^+ ($X\ ^2\Pi_g$).

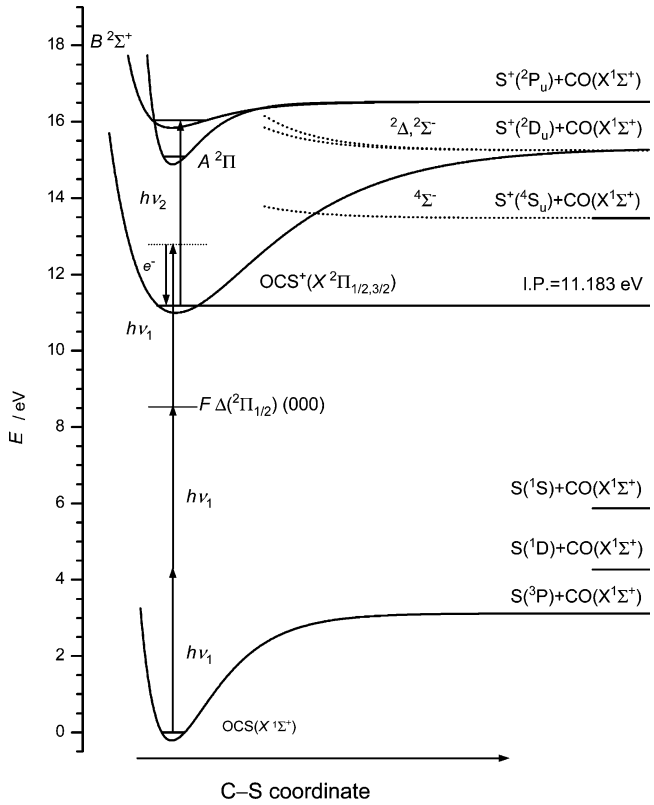

Figure 1. Schematic of potential-energy curves along the C−S coordinate (adapted from ref 4). Also illustrated are the (2 + 1) REMPI and photolysis excitation schemes used in this work.

II. Experimental Section

The experiment was conducted in a modified molecular beam apparatus.[12] About 10% of OCS seeded in He (total pressure of ∼3 atm) was expanded from an Even-Lavie valve (pulse duration of 30 μs, and 0.5 mm nozzle diameter) and skimmed to form a cold molecular beam into a second differentially pumped chamber. After passing through an 1 mm hole on the repeller plate, OCS was ionized, within a set of ion optics designed for time-sliced velocity imaging measurement,[5] by a

* To whom correspondence should be addressed. E-mail: kpliu@gate.sinica.edu.tw.

† Also Department of Chemistry, National Taiwan University, Taipei, Taiwan 106.

10.1021/jp040717z CCC: $30.25
Published on Web 01/25/2005

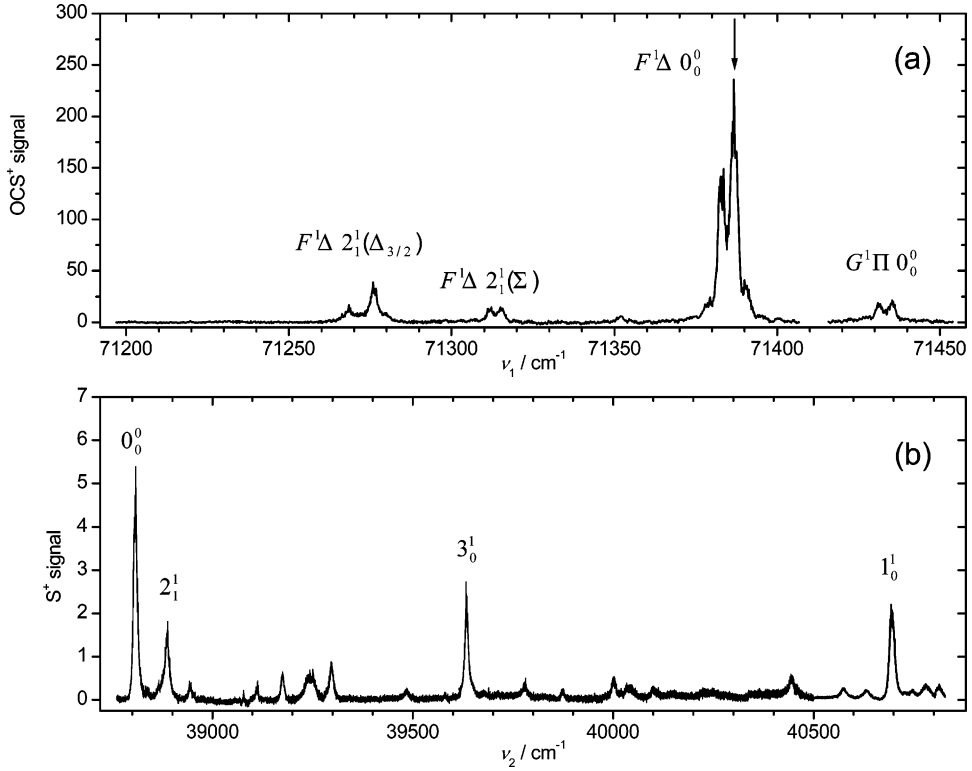

Figure 2. (a) Portion of the (2 + 1) REMPI spectrum for generating the parent ion, OCS^+. (b) Photofragment yield (S^+ cation) spectrum with the ionization laser frequency fixed at the peak of the $\tilde{F}\ ^1\Delta\ 0_0^0$ transition, indicated as an arrow in part a. The assignments of the four $\tilde{X}\ ^2\Pi \rightarrow \tilde{B}\ ^2\Sigma$ vibronic transitions used in acquiring the fragment-ion images are labeled.

(2 + 1) REMPI process via the $\tilde{F}\ ^1\Delta$ Rydberg intermediate state. (The molecular beam was directed along the ion time-of-flight axis, whereas the lasers were perpendicular to it.) By parking the ionization laser wavelength at a particular REMPI peak, the dissociation of OCS^+ cations was initiated by a second, counter-propagated laser whose wavelength was tuned to a proper $\tilde{X}\ ^2\Pi_{1/2} \rightarrow \tilde{B}\ ^2\Sigma^+$ vibronic transition.[13] The predissociated product ion S^+ was then probed using a time-sliced velocity imaging technique. A fast high-voltage switch (~30 ns duration) was pulsed to gate the gain of the Chevron-type microchannel plate (MCP) for mass selection as well as the time slicing of the ion packet. The fluorescence from a P46-phosphor was captured by a CCD camera and transferred to a computer on an every-shot basis for event counting and data analysis. Both lasers were cylindrically focused using f.l. = 50 cm lenses. To further minimize the one-color background of S^+ ions generated from the ionization laser alone, the dissociation laser was offset ~1 mm downstream from the ionization laser and delay-fired by ~600 ns to account for the traveling time of the parent ions.

It is worthwhile pointing out that a double-resonance spectroscopic scheme was exploited in this study. Although the initial (2 + 1) REMPI process already yields rather high propensity in the vibrational state selectivity of $OCS^+(\tilde{X}\ ^2\Pi_{1/2})$, the amount of contaminations from other states is not negligible, as evidenced from previous photoelectron studies.[14,15] It is the subsequent $\tilde{X}\ ^2\Pi_{1/2} \rightarrow \tilde{B}\ ^2\Sigma^+$ transition that singles out a particular upper vibronic mode/state for investigation. Because, in general, both the REMPI process and the subsequent bound-to-bound transition have their own Franck−Condon envelopes, combination of the two spectroscopies offers a flexible vehicle to access many more modes/states for studies than the IR/Raman pumping approach.

III. Results and Discussion

A small portion of the (2 + 1) REMPI spectrum of OCS is shown in Figure 2a. All spectral features can readily be assigned according to previous studies.[14−17] Figure 2b displays a photofragment (S^+) yield spectrum when the predissociation laser wavelength (λ_2) was scanned with the ionization laser (λ_1) fixed at the peak of the $\tilde{F}\ ^1\Delta\ 0_0^0$ transition, as indicated by the arrow in Figure 2a. On the basis of known vibrational frequencies,[13,18]

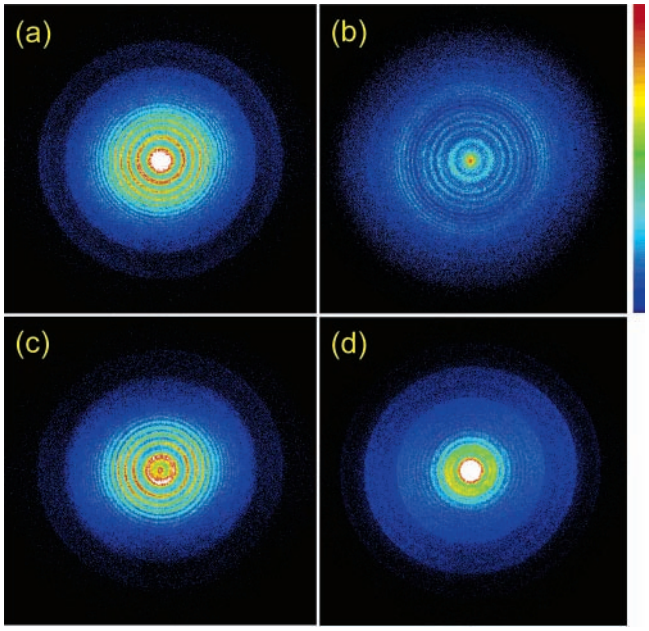

Figure 3. Time-sliced velocity-mapped images of the S^+ fragments from the state-selected OCS^+ ($\tilde{B}\ ^2\Sigma^+$) ions. The four panels correspond to the (000) level (a), (100) level (b), (010) level (c), and (001) level (d). The polarization of the photolysis laser (λ_2) is in the vertical direction. The slight anisotropy of the image arises from the nonuniformity of the detector, which was verified by a nearly identical image obtained for polarization lying perpendicular to the imaging detector.

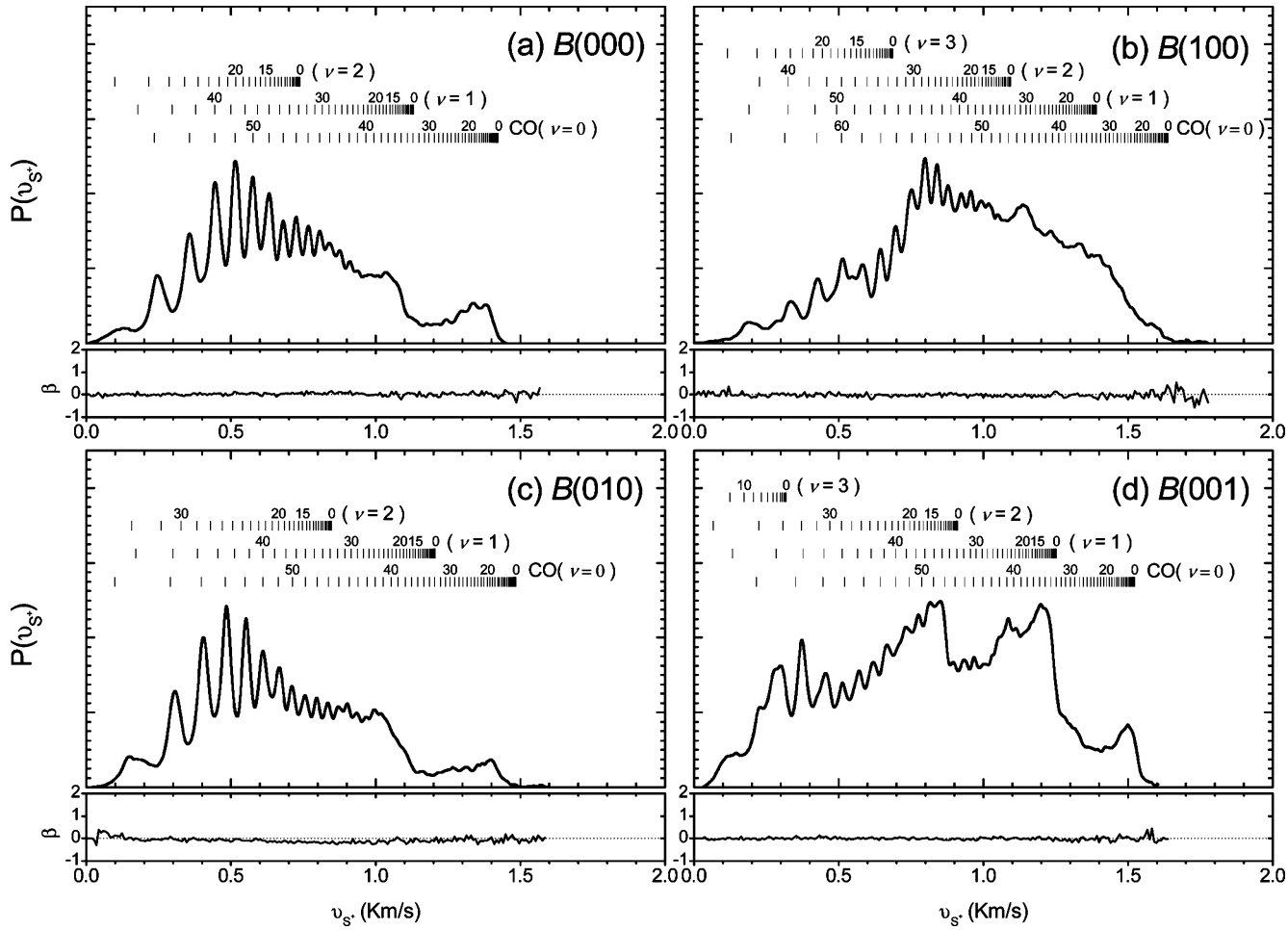

Figure 4. Product speed distributions and the anisotropic parameters (β) of the S^+ fragments. The sticks marked on top of each panel correspond to the ro-vibrational energy levels of the cofragment of CO, assuming the S^+ ion is born in the ^2D_u state.

all spectral features can be assigned to the $\tilde{X}\ ^2\Pi \rightarrow \tilde{B}^2\ \Sigma$ vibronic transitions of OCS^+. For clarity, only the four transitions reported here in acquiring the fragment-ion images are labeled.

The equilibrium structures of OCS^+ in both the ground $\tilde{X}\ ^2\Pi$ and excited $\tilde{B}\ ^2\Sigma^+$ states are of linear geometry. The three vibrational modes υ_{ss}, υ_b , and υ_{as} in the $\tilde{B}\ ^2\Sigma^+$ state have fundamental frequencies of 1870, 490, and 830 cm^{-1}, respectively.[13,18] The symmetric stretch (υ_{ss}) corresponds roughly to a local C−O stretch and the antisymmetric stretch (υ_{as}) to a local C−S vibrator. Figure 3 presents the raw images of the S^+ fragment when one quantum of each individual vibrational mode of $OCS^+(\tilde{B}\ ^2\Sigma^+)$ was excited along with that of the vibronic ground state for comparison. A casual inspection of their appearances immediately reveals some similarities as well as significant differences. All four images are dominated by a series of distinct, fine-structural rings. The strong similarity between the vibrational ground state (shown in Figure 3a) and the first bend-excited state (Figure 3c) is striking. They are in distinct variation with one quantum excitation of symmetric stretch (Figure 3b) or antisymmetric stretch (Figure 3d) of OCS^+ ($\tilde{B}\ ^2\Sigma^+$).

Analysis of the images provides more quantitative comparisons. As detailed previously,[5,19,20] a time-sliced velocity-mapped image yields directly the product density distribution in the center-of-mass (c.m.) velocity frame. To obtain the desired conventional differential cross section, $d^2\sigma/d\mu d(\cos\theta)$, a simple μ^2 weighting to the density distribution suffices. The resulted $P(\mu)$ distributions of the probed S^+ fragments and the corresponding anisotropy parameters (β) are shown in Figure 4. As indicated in Figure 1, two fragment channels are energetically accessible in this study, $S^+(^4S_u) + CO(X^1\Sigma^+)$ and $S^+(^2D_u) + CO(X^1\Sigma^+)$. The ro-vibrational energy level sticks marked on top of each panel are based on the assumption that the cofragment S^+ is born in the ^2D_u state. As can be seen, it is entirely consistent with the experimental data. Even the fine-spaced peaks can readily be assigned to the high-j levels of the $CO(\upsilon = 0, j) + S^+(^2D_u)$ fragment pair, except for the (001) $B^2\Sigma^+$ predissociation where the high-j levels of $CO(\upsilon = 1, j) + S^+(^2D_u)$ may also make a significant contribution. In terms of the fraction of translational energy release, they are 29%, 37%, 24%, and 35% for the (000), (100), (010), and (001) predissociating states, respectively. As to the product angular distribution, all four cases display an isotropic one ($\beta \approx 0$), as anticipated, in general, for a slow predissociation process. The very slight negative β value for the (010) state is likely within our measurement errors. More precise measurement will be needed. Due to the heavy overlap of the ro-vibrational features, unfortunately, it is impossible to quantitatively determine the CO-fragment ro-vibrational distributions. Nonetheless, the onset of each CO vibrational level is apparent. Hence, qualitatively one can conclude that the coincident CO fragments (to the $S^+(^2D_u)$ product) are formed with significant vibrational excitation, and for the low vibrational states, particularly $\upsilon = 0$, the CO are characterized by very high rotational excitations.

Hubin-Franskin et al.[21] were the first to perform a detailed study on the decay of the OCS^+ cations from a dissociative photoionization process. In that study the ions were produced by photoionization of OCS with synchrotron radiation in the

13.5−16.5 eV range. The predissociation dynamics was investigated by a threshold photoelectron−photoion coincidence spectroscopic technique. It was concluded that the fate of the $\tilde{B}\ ^2\Sigma^+$ state, similar to the $\tilde{A}\ ^2\Pi$ state, is predominantly a nonradiative decay to the ground $\tilde{X}\ ^2\Pi$ state, followed by a crossing to the $^4\Sigma^-$ surface, leading to the major product channel of $S^+(^4S_u) + CO(X^1\Sigma$, high $v)$. A minor channel of $S^+(^2D_u) + CO(X^1\Sigma)$ was also inferred from a small feature in the TOF data. Similar experimental results were obtained later by Morse et al.[22] Owing to the limited resolution, however, the state assignments of both the predissociating parent ion and the fragment channels in these works were not without ambiguity. In the present study, the initial state selection was governed by a double-resonance excitation scheme and the fragment state assignment deduced from a high-resolution product image was made with rotational resolution. Contrary to the previous conclusion,[21,22] we found that all fragmentations are associated with the $S^+(^2D_u) + CO(X^2\Sigma^+)$ channel—no sign of the formation of $S^+(^4S_u) + CO(X^2\Sigma^+)$, which clearly excludes the role of the spin−orbit coupling in this predissociation process.

As depicted in Figure 1, both $\tilde{B}\ 2\Sigma^+$ and $\tilde{A}\ ^2\Pi$ states correlate asymptotically to the $S^+(^2P_u) + CO(X^1\Sigma)$ pair, whereas the ground $\tilde{X}\ ^2\Pi$ state correlates to the $S^+(^2D_u) + CO(^1\Sigma^+)$ limit. The latter also leads to two repulsive surfaces of the $^2\Sigma^-$ and $^2\Delta$ symmetries that can cross the $\tilde{A}\ ^2\Pi$ and $\tilde{B}\ ^2\Sigma^+$ states at shorter C−S distances. From symmetry arguments,[23] the predissociative states of this study are vibronically of $^2\Sigma^+$ symmetry for (000), (100), and (001) states and of $^2\Pi$ symmetry for (010); thus, they cannot couple directly to these two repulsive surfaces. On the other hand, the internal conversion of $\tilde{B}\ ^2\Sigma^+ \rightarrow \tilde{X}\ ^2\Pi$ through nonadiabatic transitions could be facile. The internally hot molecules of $\tilde{X}\ ^2\Pi$ can then undergo unimolecular decomposition adiabatically, leading to the production of $S^+(^2D_u) + CO(X^1\Sigma^+)$. This is likely a reaction pathway responsible for the observation.

Yet, the variation of the patterns of the fragment kinetic energy release shown in Figure 4 suggests more than just one dissociation mechanism. A conceivable candidate is that the initial vibronic state is coupled to the $\tilde{A}\ ^2\Pi$ state that then crosses to the repulsive $^2\Delta$ surface for dissociation. As hinted in Figure 1, there could be a crossing between $\tilde{B}\ ^2\Sigma^+$ and $\tilde{A}\ ^2\Pi$ states which lies about 1 eV above the $\tilde{A}\ ^2\Pi$ ground state in the inner wall of the C−S coordinate, in a linear configuration.[20] As OCS^+ bends, $\tilde{B}\ ^2\Sigma^+$ transforms into A′ symmetry and $\tilde{A}\ ^2\Pi$ splits into A″ and A′ symmetries. The two A′ surfaces will avoid each other, forming a conical intersection.[23] Hence, the $\tilde{B}\ ^2\Sigma^+ \rightarrow \tilde{A}\ ^2\Pi$ nonadiabatic transition could proceed through the conical intersection that serves as an effective funnel in guiding the intramolecular dynamics.

In other words, we assert that there are two facile pathways: $\tilde{B}\ ^2\Sigma \rightarrow \tilde{X}\ ^2\Pi \rightarrow$ fragments and $\tilde{B}\ ^2\Sigma \rightarrow \tilde{A}\ ^2\Pi \rightarrow\ ^2\Delta \rightarrow$ fragments. (The latter can, of course, also branch out microscopically as $\tilde{B}\ ^2\Sigma \rightarrow \tilde{A}\ ^2\Pi \rightarrow \tilde{X}\ ^2\Pi \rightarrow$ fragments. We are not able to distinguish it from the former on the available experimental data.) While both predissociative pathways involve internal hot molecules as intermediates, the former undergoes a presumably barrierless unimolecular decomposition and the latter will eventually evolve on a repulsive surface as the two fragments fly apart, which can result in higher kinetic-energy release. Experimentally, we found that the averaged kinetic-energy releases from (100) and (001) are significantly larger than the other two, (000) and (010). Furthermore, the product kinetic-energy distribution from the vibronic ground state is strikingly similar to that from the (010) $\tilde{B}\ ^2\Sigma$ state, suggestive of the identical mechanism. One plausible way to rationalize these observations is that the $\tilde{B}\ ^2\Sigma \rightarrow \tilde{A}\ ^2\Pi$ conical intersection lies slightly above the first bend-excited state of $\tilde{B}\ ^2\Sigma$, i.e., between 1.02 and 1.06 eV above the $A\ ^2\Pi$ state, thus essentially shutting off this pathway for both (000) and (010) states. On the other hand, the above two pathways can contribute to the predissociation of the (100) and (001) $B\ ^2\Sigma$ states so that their fragment $P(\mu)$ distributions comprise of both components and possibly the interferences, resulting in more complicated patterns.

In summary, an incisive and versatile experimental approach is exemplified here to unravel the mode-specific predissociation dynamics. In this approach a double-resonance spectroscopic scheme is exploited to select a particular mode or state. A time-sliced velocity imaging technique maps the subsequent predissociation dynamics. The combination of these two techniques is quite versatile and could have a wide range of variants and applications. As demonstrated in the present $OCS^+(\tilde{B}\ ^2\Sigma)$ study, it enables us to examine the dynamical consequences from all three different vibration modes. A significant mode dependence, i.e., mode-specific memory is retained despite the long dissociation time, was found. A qualitative interpretation is proposed which awaits further theoretical investigations. Studies of higher vibronically excited states, including the quasi-bound states lying above the $S^+(^2P_u) + CO(X^1\Sigma^+)$ asymptote, are in progress and will be reported in the future.

Acknowledgment. This work was supported by the National Science Council of Taiwan (NSC 93-2113-M-001-041). Helpful discussion with Dr. J. J. Lin is gratefully acknowledged.

References and Notes

(1) Crim, F. F. *Annu. Rev. Phys. Chem.* **1993**, *44*, 397. Crim, F. F. *Acc. Chem. Res.* **1999**, *32*, 877 and references therein.
(2) Zare, R. N. *Science* **1998**, *279*, 1875 and references therein.
(3) Bar, I.; Rosenwaks, S. *Int. Rev. Phys. Chem.* **2001**, *20*, 711 and references therein.
(4) Delwiche, J.; Hubin-Franskin, M.-J.; Guyon, P.-M.; Nenner, I. *J. Chem. Phys.* **1981**, *74*, 4219.
(5) Lin, J. J.; Zhou, J.; Shiu, W.; Liu, K. *Rev. Sci. Instrum.* **2003**, *74*, 2495.
(6) Yang, B.; Chiu, Y.; Fu, H.; Anderson, S. L. *J. Chem. Phys.* **1991**, *95*, 3275.
(7) Yang, B., Chiu, Y.; Anderson, S. L. *J. Chem. Phys.* **1991**, *94*, 6459.
(8) Boesl, U. *J. Phys. Chem.* **1991**, *95*, 2949.
(9) Weinkauf, R.; Boesl, U. *J. Chem. Phys.* **1994**, *101*, 8482.
(10) Cha, Ch.; Weinkauf, R.; Boesl, U. *J. Chem. Phys.* **1995**, *103*, 5224.
(11) Beckert, M.; Greaves, S. J.; Ashfold, M. N. R. *Phys. Chem. Chem. Phys.* **2003**, *5*, 308.
(12) Hsieh, C.-H.; Lee, Y.-S.; Fujii, A.; Lee, S.-H.; Liu, K. *Chem. Phys. Lett.* **1997**, *277*, 33.
(13) Kakoschke, R.; Boesl, U.; Hermann, J.; Schlag, E. W. *Chem. Phys. Lett.* **1985**, *119*, 467.
(14) Weinkauf, R.; Boesl, U. *J. Chem. Phys.* **1993**, *98*, 4459.
(15) Yang, B.; Eslami, M. H.; Anderson, S. L. *J. Chem. Phys.* **1988**, *89*, 5527.
(16) Morgan, R. A.; Baldwin, M. A.; Ascenz, D.; Orr-Ewing, A. J.; Ashfold, M. N. R.; Buma, W. J.; Milan, J. B.; Scheper, C. R.; Lange, C. A. de. *Int. J. Mass. Spectrom. Ion Processes* **1996**, *159*, 1.
(17) Berger, J. Ph.; Baker, J.; Couris, S. *J. Chem. Phys.* **1996**, *105*, 6147.
(18) Chen, W.; Hochlaf, M.; Rosmus, P.; He, G. Z.; Ng, C. Y. *J. Chem. Phys.* **2002**, *116*, 5612.
(19) Gehardt, C. R.; Rakitzis, T. P.; Samartzis, P. C.; Ladopoulos, V.; Kitsopoulos, T. N. *Rev. Sci. Instrum.* **2001**, *72*, 3848.
(20) Townsend, D. A.; Minitti, M. P.; Suits, A. G. *Rev. Sci. Instrum.* **2003**, *74*, 2530.
(21) Hubin-Franskin, M. J.; Delwiche, J.; Guyon, P. M.; Richard-Viard, M.; Lavollée, M.; Dutuit, O.; Robbe, J. M.; Flament, J. P. *Chem. Phys.* **1996**, *209*, 143.
(22) Morse, S.; Takahashi, M.; Eland, J. H. D.; Karlsson, L. *Int. J. Mass. Spectrom.* **1999**, *184*, 67.
(23) Herzberg, G. *Molecular Spectra and Molecular Structure III*; Van Nostrand C., Inc.: Holland 1966.